Using Pulsed Power for Hydrodynamic Code Validation

Randall J. Kanzleiter, Walter L. Atchison, Richard L. Bowers, Richard L. Fortson, Joyce A. Guzik, Russell T. Olson, John L. Stokes, and Peter J. Turchi, *Fellow, IEEE*

***Abstract*—As part of ongoing hydrodynamic code verification and validation efforts, a series of near-term liner experiments (NTLX) was designed for the Shiva Star capacitor bank at the Air Force Research Laboratory [1]. An aluminum liner that is magnetically imploded onto a central target by self-induced Lorentz forces drove the experiments. Target design utilized the adaptive mesh refinement Eulerian hydrodynamics code radiative adaptive grid eulerian (RAGE) in two- and three-dimensional. One-dimensional simulations of the liner driver utilizing the lagrangian magnetohydrodynamics code RAVEN are used to set the initial temperature and density profiles as well as liner velocity at impact time. During liner/target impact, a convergent shock is generated in the target that drives subsequent hydrodynamics experiments. In concentric targets, a cylindrically symmetric shock will converge on axis. The degree of shock symmetry observed characterizes the liner symmetry at impact. By shifting the target center away from the liner driver axis, variations in shock propagation velocity generate off-center shock convergence. Results indicate that RAVEN and RAGE are in excellent agreement for the calculated shock trajectory. However, a small but significant discrepancy does occur during the last few millimeters of run-in when convergence effects are greatest. The codes predict shock arrival times that are approximately 100 ns faster than those observed experimentally.**

***Index Terms*—Code validation, convergent shocks, hydrodynamics, pulsed power.**

I. Introduction

With the increased reliance on numerical simulation for dynamical problems in complex geometries, questions arise as to the credibility of the results produced. Traditional approaches focus on comparing computer simulations with simple [usually one-dimensional (1-D)] problems for which exact solutions exist. While this approach is a necessary first step, it does not guarantee that good agreement between computation and theory will extend to even the simplest multidimensional hydrodynamic flows. A collaborative program involving the Los Alamos National Laboratory (LANL) and the Air Force Research Laboratory (AFRL) designed simple multidimensional hydrodynamic experiments utilizing the Shiva Star pulsed-power machine in order to validate hydrodynamic codes of general interest. These experiments were to obtain high-quality data characterizing hydrodynamic phenomena induced in simple convergent geometries that cannot be calculated analytically. The first of these experiments, the near-term liner experiments (NTLX) series, is reported here.

The experiments were designed using the adaptive mesh refinement (AMR) Eulerian hydrodynamics code RAGE (Radiative Adaptive Grid Eulerian) [2], [3]. Since RAGE lacks the electromagnetic effects needed to consistently model pulsed power magnetic drives such as Shiva Star, the 1-D Lagrangian code RAVEN [4], [5] was used to model magnetohydrodynamics (MHD) effects and to set the initial liner/target interaction parameters for use in RAGE.

The initial NTLX experiment consisted of a symmetric liner/target configuration to produce a uniform and concentric shock with axial convergence. Subsequent shots explored both central and off-center shock propagation and measured shock trajectories through target materials by offsetting the acrylic core, initially by 4 mm, from the liner driver axis. RAGE simulations of the Sn/acrylic target predict that impact of the imploding aluminum driver with the outer Sn target generates a cylindrical shock with pressures exceeding 1 Mbar in the Sn and a point of shock convergence offset from the acrylic target's center when an offset target is used. Axial radiography was used to determine the geometry of the converging shock along with location of shock convergence and the Sn/acrylic interface position.

Although more complex target geometries are being designed, the ability to accurately model shock dynamics near axis for simple convergent geometries or small shock convergence offsets represents a crucial first step in the study of hydrodynamic flows. Furthermore, it is important to identify any diagnostic limitations in the pulsed power regime that may affect the study of more complex targets.

II. Experiment Arrangement

The NTLX experimental series employed a previously characterized cylindrical aluminum liner driver that is magnetically imploded onto a central target (Fig. 1). Prior studies and experiments have shown that such liners represent an ideal source of highly cylindrical drivers possessing a well-characterized center of convergence. The solid liner driver is shocklessly accelerated by the induced magnetic field. Liner velocity at impact is controlled in part by variations in bank voltage or the mass of the liner driver. This allows one to "tune" the impact velocity in order to generate shocks of various strengths. The liner also acts to shield the inner target from the magnetic field and currents that drive it as well as to allow for a relatively large central volume in which to carry out and diagnose experiments

Manuscript received September 26, 2001; revised August 30, 2002. This work was supported in part by the U.S. Department of Energy, by the University of California, by the Los Alamos National Laboratory under Contract W-7405-Eng-36, and by Contract LDRD/DR—Next Generation Sophistication in Defense and High Energy Density Exploratory Research (99524).

The authors are with the Los Alamos National Laboratory, Los Alamos, NM 87545 USA (e-mail: kanzlr@lanl.gov).

Digital Object Identifier 10.1109/TPS.2002.806641

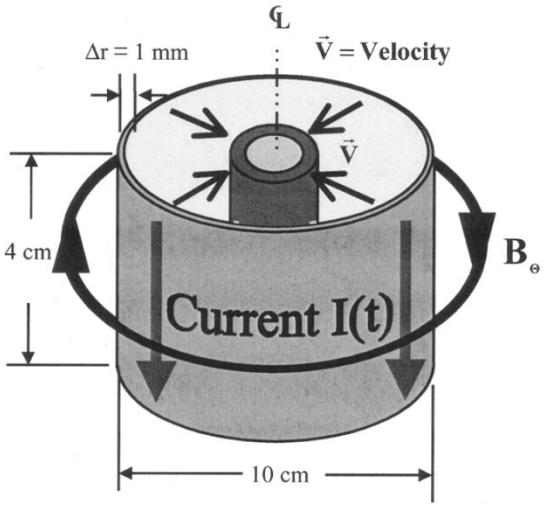

Fig. 1. Pulsed-power implosion relies on the self-induced Lorentz force to generate high liner velocities just prior to impact. Liner/target impact subsequently launches a shock into the target material.

[6]. Early results showed that the drive conditions accelerating the solid liner are well represented by 1-D MHD treatments. Following the onset of current flow, the self-induced radial Lorentz force accelerates the 1-mm-thick aluminum liner to a radial velocity of 6.25 mm/μs at a target radius of 2 cm. The convergent shock generated at liner/target impact drives subsequent hydrodynamic experiments characterizing shock behavior in symmetric and asymmetric geometries. Target arrangements for both of these configurations are shown in Fig. 2(a) and (b). In the concentric target arrangement [Fig. 2(a)], a cylindrically symmetric shock will converge on axis. This self-characterizes the symmetry of the liner driver and the concentricity of the target assembly. By shifting the center of the core away from the liner driver's center of convergence [Fig. 2(b)], off-center shock convergence is produced. The outer target layer consists of a tin casing material used to isolate shock convergence effects from the magnetic drive. For shock pressures greater than $\sim$300 kbar the outer tin target melts, thereby removing complications due to strength effects from comparisons. Simulations indicate that liner/target interaction in the NTLX generated shock pressures in excess of 1 Mbar in the tin; well above the 300 kbar shock pressure necessary for the solid–liquid phase transition.

The Shiva Star pulsed power facility located at the AFRL generates the MHD drive used to accelerate the aluminum liner. Shiva Star is a cylindrically symmetric, capacitively driven pulsed power source that generates a 16-MA current with a 10-μs quarter-cycle rise time. Drive conditions following bank discharge are determined by the RAVEN MHD code. In RAVEN, the Shiva Star bank is represented as seen in Fig. 3 as a lumped-parameter circuit with a specified capacitance and voltage drop across the capacitor. Impact conditions determined by RAVEN are then used as initial conditions for the hydrodynamic simulations. Comparison of the measured and RAVEN generated current profiles in Fig. 4 shows excellent agreement until shortly after liner/target impact occurs.

Liner/target impact is diagnosed by B-dot probes and the subsequent shock motion is followed with axial and radial radiography. A set of six symmetrically arranged B-dot loops measuring current fluctuations, dI/dt, provides information on impact timing and symmetry. The liner at target impact is found to retain a circular cross section with only a slight shift in the liner axis. Displacements of the liner driver axis from the target center are displayed in Table I for the NTLX series. Distances of this size correspond to liner symmetries, $\Delta r/r$, of between 97.5% to better than 99.0% at an impact radius of 2 cm. Liner behavior in the cylindrical R–Z plane is found to be equally as good, as seen in Fig. 5. Radial radiographs for NTLX-2 indicate that the liner retains a straight and uniform character just prior to impact. A slight "foot" is observed near each end due to liner/glide plane interactions. However, this is found not to influence the dynamics of the shock motion or affect diagnostic measurements. The radiographed "foot" generates a small disturbance just prior to impact of the main liner, but releases waves near the ends of the impact region weaken and slow the shock near the liner edge. Axial radiography is used to track shock motion following breakout from the Sn/acrylic interface. Four X-ray diodes are located below the target generating X-ray pulses that interact with a sodium–iodide scintillator located above the target area. The image is then piped to a 4-frame camera that records the shock motion. With a 700-ns time response of the scintillator material, it is possible to obtain a maximum of three images during the shock convergence phase of the implosion.

III. Computational Approach

Two codes, RAVEN and RAGE, were used to provide a complete simulation of shock generation and convergence in the cylindrical geometries employed in the NTLX series. Two separate codes were used to avoid limitations imposed by either independent simulation. RAGE calculations lack consideration of MHD effects and strength issues, while RAVEN is limited to 1-D simulations of the symmetric target arrangement. In this manner, target design calculations were performed using RAGE to investigate multidimensional effects with RAVEN providing impact conditions generated by the MHD acceleration of the liner driver. Details of these codes as they affect the design and analysis of the NTLX experiments are considered next.

A. RAVEN and Circuit Modeling

RAVEN is a 1-D Langrangian MHD code utilizing artificial viscous stresses to represent shocks and SESAME [7] equation-of-state data to model the liner driver and subsequent shock evolution through the NTLX target. The code solves the RLC circuit shown in Fig. 3 to produce the acceleration of the liner driver. The time-dependent resistance $R(t)$ in Fig. 3 simulates an attached safety fuse that prevents damage to the capacitor bank associated with current reversal. The circuit model self-consistently calculates the coupling between the pulsed power system and the imploding liner driver. RAVEN also includes a Steinberg–Guinan [8] strength model along with a tabular melt model for the aluminum liner driver. SESAME resistivity data is used to complete the circuit model and determine the liner state (density, temperature, and velocity) at impact. These state parameters are then used as initial conditions for multidimensional hydrodynamic calculations of the target using RAGE.

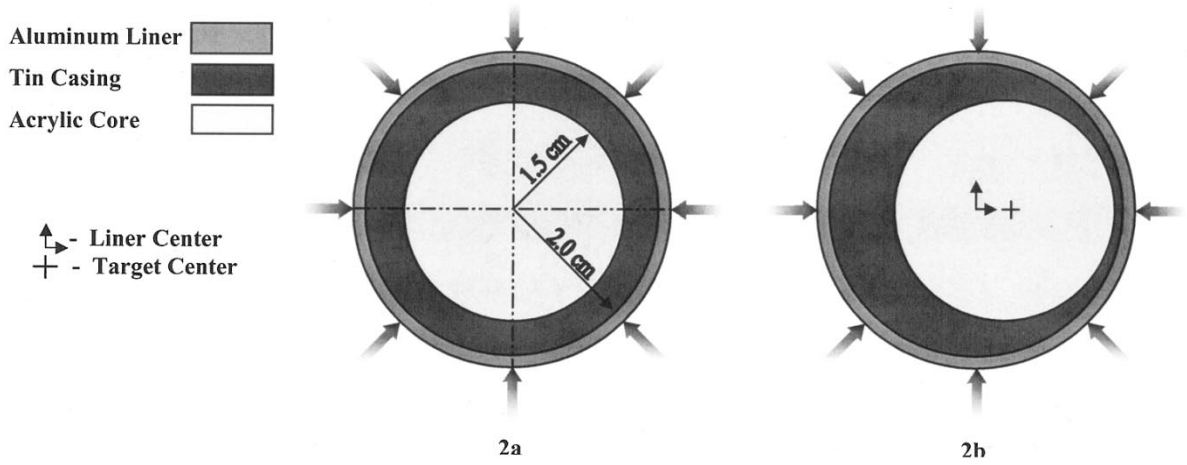

Fig. 2. Target arrangements used in NTLX liner implosion experiment. (a) Symmetric target configurations. (b) Asymmetric target configurations.

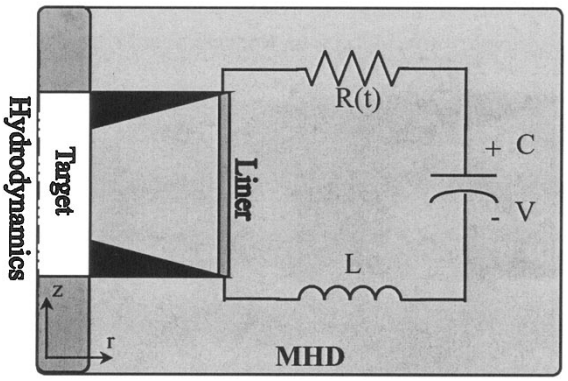

Fig. 3. Lumped-parameter circuit model for the NTLX series including Shiva Star operational parameters. ($C = 1300$ μF, $V = 82$ kV, $L = 26.3$ nH, $R = 0.5$ mΩ).

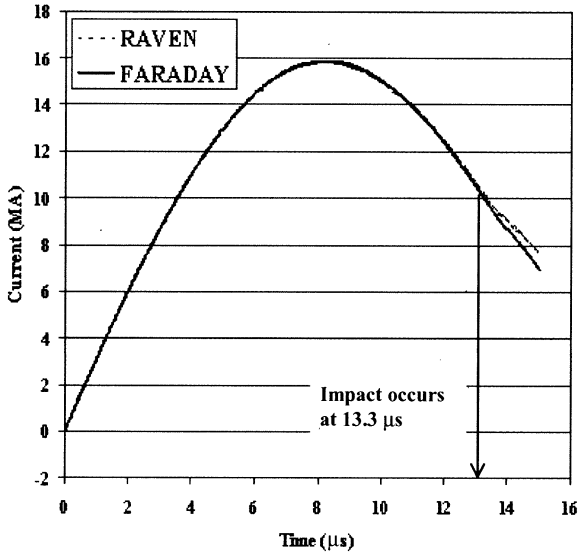

Fig. 4. RAVEN calculations using the lumped-parameter circuit model show excellent agreement with experimental measurements made by faraday detectors until after liner/target impact.

The RAVEN circuit model was already shown to be capable of reproducing the Shiva Star drive current. In addition to direct calculations of the circuit current, RAVEN generates a simulated B-dot signal for direct comparison with experimental data. Information from the azimuthal probes are time averaged to produce a single average B-dot signal to compare with the 1-D RAVEN results. This timing comparison is presented in Fig. 6, which shows a high level of agreement in the arrival time, within a few nanoseconds, of the calculated and measured signals. Variations in impact timing from the ideal symmetric case reduce the experimentally measured signal amplitude below the 1-D RAVEN result, while maintaining a similar signal shape. There is also evidence that the calculated signal is extremely sensitive to bank charge voltage. Less than a 1% variation in the assumed voltage easily produces a shift of 100 ns in the calculated probe signal. At present, initial voltage settings are uncertain by approximately $\pm 1.5\%$; this represents a limitation on the absolute timing of our experiments. We note that despite this absolute uncertainty, relative timing is more accurately known. Although the impact timing appears to be quite sensitive to the details of the bank operation, calculations of the liner state at impact are more robust. The liner state at impact is determined by the total electrical action $Q(t)$, associated with liner acceleration. This quantity is far less sensitive to bank details as seen in

$$Q(t) = \int_0^t j^2(\tau)\, d\tau \tag{1}$$

where $j(\tau)$ is the current density acting through the liner.

Even with a careful matching of B-dot signals, experimental criteria that determine the absolute timing of liner/target impact remain undetermined. However, it is possible to make comparisons based on estimated collision times. A collision between

TABLE I
SHIFT IN LINER DRIVER CONVERGENCE CENTER AS MEASURED BY B-DOT PROBES DURING THE NTLX SERIES

Shot #	Signal Spread (ns)	Center Shift (mm)
NTLX-1	123	0.384
NTLX-2	43	0.134
NTLX-3	77	0.240
NTLX-4	26	0.081

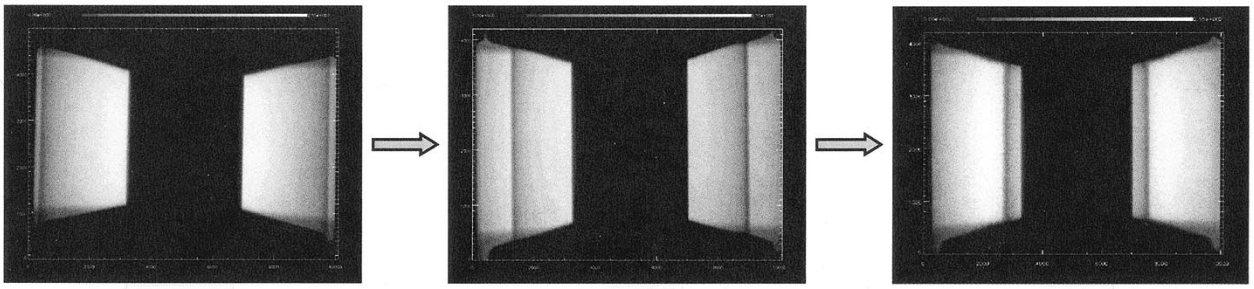

Fig. 5. Radial radiographs of the imploding liner during NTLX-2 show few signs of liner perturbation. (a), (b), and (c) correspond to 0.0, 9.413, and 12.666 μs, respectively.

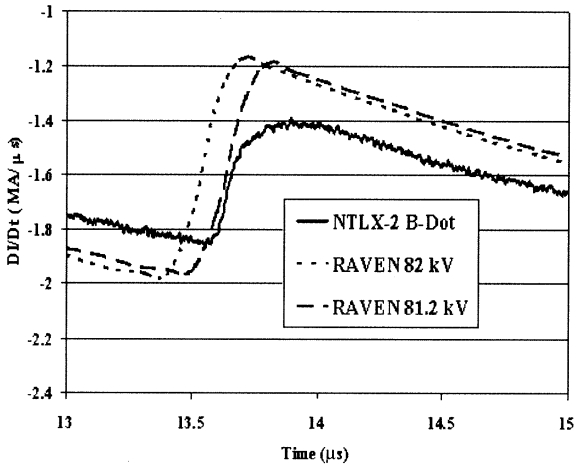

Fig. 6. RAVEN closely models the arrival time of the experimentally determined B-dot signal. However, simulation results remain highly sensitive to initial voltage with a $<$1% change in initial voltage producing a 100-ns change in impact timing.

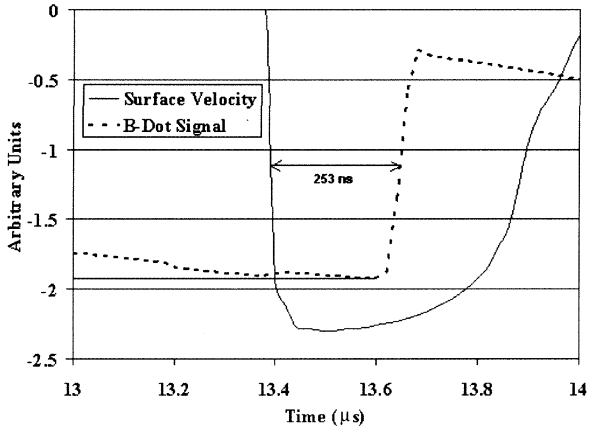

Fig. 7. Once liner/target impact occurs, it takes 253 ns to generate the resulting B-dot signal.

the liner and target produces a large dL/dt, which generates a small (though detectable) change in the B-dot data. Correlating the arrival of the B-dot jump with liner/target impact is complicated by the finite time interval required for the collision to produce a measurable probe response. At collision, an outgoing shock is transmitted through the impacting aluminum liner. When the outbound shock slows the portion of the liner containing the majority of the current, the sudden dL/dt manifests itself as the B-dot jump. In order to estimate the experimental impact time from available data, RAVEN is used as in Fig. 7 to determine the simulated time between the onset of outer surface motion in the central target (signaling impact) and the arrival of the B-dot signal. RAVEN estimates a delay of 253 ns between the time the target is struck by the liner and the arrival of the simulated B-dot jump. Applying this 253-ns delay to the arrival of the measured B-dot signal estimates the experimental impact time. Later data comparisons between simulation and experiment are made relative to this estimated time of impact.

B. RAGE and Hydromodeling

The RAGE code is a 1-D, two-dimensional (2-D), or three-dimensional (3-D), multimaterial Eulerian hydrodynamics code utilizing adaptive mesh refinement (AMR) and either analytical or SESAME equation of state information. The adaptive meshing employed in RAGE allows the code to continuously rezone by dividing or combining cells as necessary to enhance computational efficiency. At material boundaries or in regions of high gradients between hydrodynamic variables, the grid refines to capture shock or material motion. Explicit interface tracking is not included in RAGE. Material diffusion across the interfacial region is limited by using the highest allowable level of zone refinement in these regions. Calculation of hydrodynamic shocks is handled by a second-order piecewise linear Godunov method.

The RAGE results for the NTLX series presented here start with an initial 1-mm grid resolution with five levels of allowable refinement for a minimum zoning of 0.0625 mm. This minimum zoning is set by the criteria that the shock center of convergence be invariant as the grid resolution is increased. Fig. 8 shows a section of a RAGE grid in the vicinity of a converging shock. The disturbance introduces high gradient regions where the grid automatically refines in advance of the incident shock. In regions far removed from the recently shocked material, the grid eventually dezones to lower resolutions wherever possible. One challenge encountered in the current configuration is the effect of shock convergence on grid adaptation. Radial gradients in these geometries remain sufficiently high to prevent relaxation of the computational grid. Only in regions far removed from the convergence center do gradients diminish sufficiently to allow dezoning. This mitigates some of the computational savings realized through grid adaptation. However, prior to shock passage grid, resolution remains coarse thereby reducing computational effort.

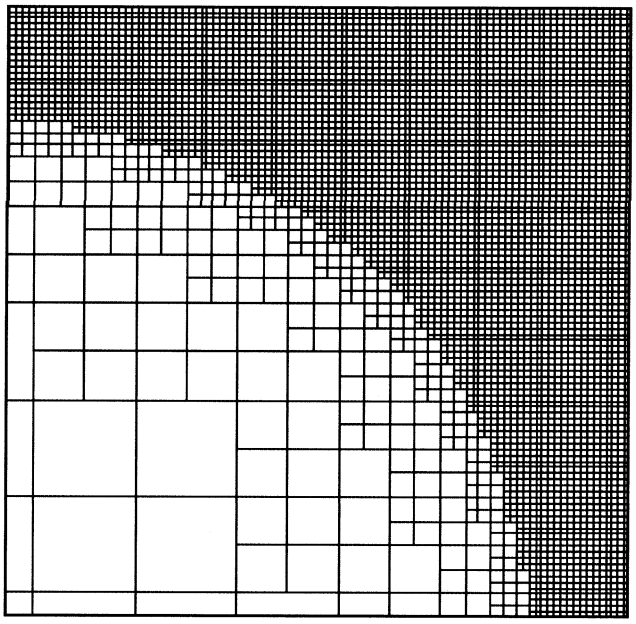

Fig. 8. Section of a RAGE grid showing adaptation of the AMR computational grid in the presence of a hydrodynamic shock. The shock boundary is located several zones into the region of highest refinement.

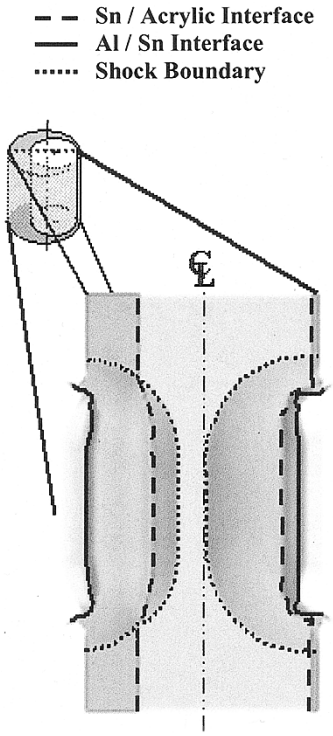

Fig. 9. An axial slice along the symmetry plane of a 3-D asymmetric RAGE simulation shows that a significant portion of the shock retains a straight and uniform character until central convergence.

RAGE simulations were employed in two modes during these validation efforts. Two-dimensional axial slices through the target mid-plane on a Cartesian grid structure were used to determine the location of shock convergence and to provide diagnostic timing information. Effects due to shock curvature along the liner driver's symmetry axis were investigated through 3-D Cartesian simulations along with 2-D RZ simulations in cylindrical geometry for the symmetric target. Fig. 9 is a RZ slice through the symmetry plane in a 3-D asymmetric target simulation. In three dimensions, disturbances propagating inward from the liner ends cause a weakening and, therefore slowing of the shock as it converges on axis. It is significant to note that by the time the shock has fully converged on axis, an approximately 1.5-cm-wide shocked region remains straight and uniform on axis. This eases diagnostic interpretation, and comparisons between simulation and experimental data are thus limited to a case of a uniform strength convergent shock.

IV. Results

Besides design and diagnostic timing calculations, RAVEN and RAGE provide shock trajectories and interfacial boundary data for the symmetric (experiments NTLX-1 and NTLX-3) and asymmetric (experiments NTLX-2 and NTLX-4) target configurations. This shock and interface data, as well as measurements of the shock center of convergence in the asymmetric experiments provides the necessary data for these code validation efforts.

As discussed in Section III-B outlining RAVEN operation, the relative timing of the simulated and experimental data points is very sensitive to the details of the MHD drive behavior. Small differences in the initial bank conditions can result in significant variations in the liner/target impact times as measured by the B-dot probes with little variation in the liner state at impact. With this in mind, all simulated and experimental data are compared using the respective liner/target impact as an initial reference time instead of time since current start.

Computationally, the determination of impact time is straightforward in both codes since this process is directly observable. However, resolving the experimental impact requires adjusting the average B-dot signal by the simulated delay between impact and generation of the diagnostic signal. This provides only indirect timing of the true liner/target impact. Fig. 7 showed this effect through the 253-ns delay between the onset of the target surface motion and the subsequent generation of the B-dot signal. The level of uncertainty associated with using a simulated delay in order to determine the experimental impact time remains unresolved since no precise experimental measure of impact time was recorded. A further complication in fixing the experimental impact time is the small but measurable offset in the liner driver axis at collision. The liner implosions are highly symmetric, yet a small but measurable difference is seen in the relative timing of the six separate B-dot signals. Table I shows the timing differences between the first and last B-dot signal received in each experiment during this series. This signal spread indicates that the experimental liner/target impact takes between 26 and 123 ns to complete once initial contact is achieved. Unlike the computational results, liner/target impact is not an instantaneous occurrence.

A. Symmetric Target: [Fig. 2(a)]

This configuration allows a direct comparison between the RAVEN calculations including the MHD drive and RAGE 2- and 3-D hydrodynamic runs. Comparisons of the simulated shock trajectory and the experimentally determined shock

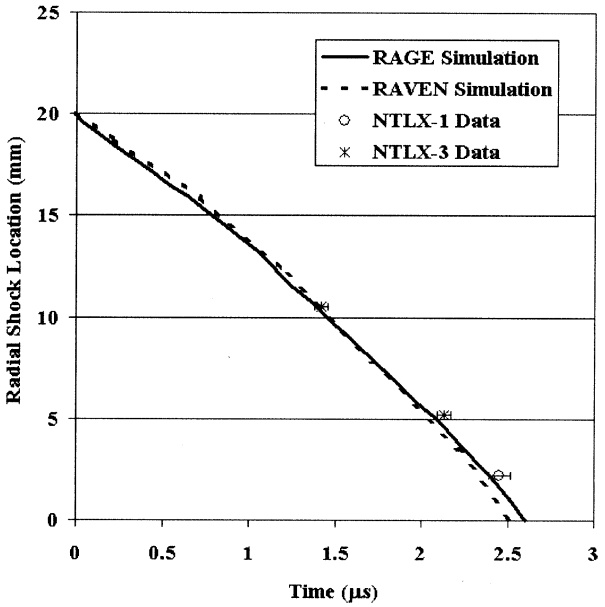

Fig. 10. Both simulation and experimental data show a high level of agreement for the measured shock location. Comparisons between RAGE and RAVEN show the greatest discrepancy near axis where convergence effects dominate.

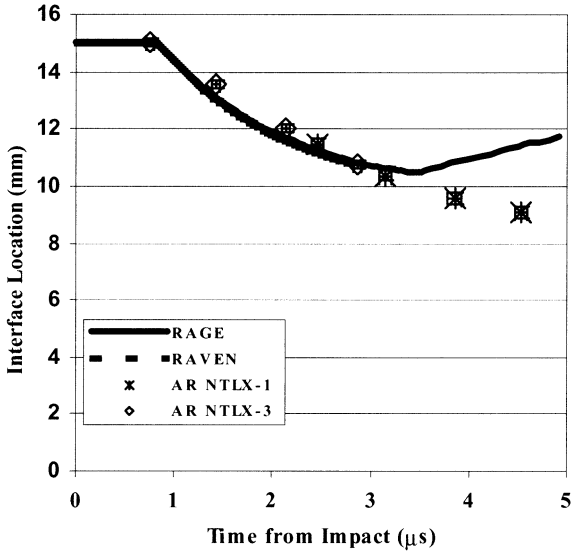

Fig. 11. RAVEN and RAGE produce indistinguishable behavior of the material interface with and without strength effects. The radiographed interface exhibits a slightly lower compression rate than that calculated. The divergence at 3.5 μs is due to calculated shock interface interactions that are not experimentally observable.

location are presented in Fig. 10. Although based on different solution techniques, RAVEN and RAGE results exhibit excellent agreement over most of the shock trajectory. The only significant difference between the simulations occurs during the final few millimeters of the implosion process where convergence effects become important. As the shock waves coalesce on axis, RAVEN indicates a greater influence of convergence on the shock trajectory.

Besides the shock trajectory, the temporal evolution of the Sn/acrylic interface provides a second data set used in this study. The NTLX series was designed to use an outer Sn target to isolate the MHD drive from the hydrodynamic motion generated in the target at liner impact. This isolation occurs since the time scale of the shock motion is much faster than the diffusion of the magnetic field through the outer Sn target. Strength effects were presumed to be inconsequential since Sn melts for shock pressures greater than approximately 300 kbar and impact of the NTLX liner generates calculated shock pressures greater than 1 Mbar. Fig. 11 illustrates this point as RAVEN simulations including a Steinberg–Guinan strength model and RAGE simulations without strength produce identical results for the interface position as a function of time. RAVEN simulations terminate at 3 μs following impact, which is well after central convergence at 2.5 μs. RAGE computations were run further to compare with late time experimental data (up to 5 μs following liner/target impact).

Comparisons between simulated and experimental interface data show that both RAVEN and RAGE initially predict a higher interface velocity than is observed. As the system evolves, the simulated motion of the interface slows to a greater extent than the experimental observation. This behavior is seen both in RAGE (which lacked strength) and in the RAVEN computational model that included material strength. Evident in Fig. 11 is a divergence between simulated and measured interface location 3.5 μs following impact. Computationally, this motion is observed when the converging shock reflects on axis and passes back through the material interface, reversing its direction. This effect is not observed radiographically since the high density of Sn and 3-D parallax effects allow imaging of only the upper edge of the Sn/acrylic interface. The 3-D simulation of Fig. 9 illustrates this effect of shock curvature. Since the mid-plane motion is not experimentally observable in the current geometry, comparisons of simulated and measured interface locations are limited to times before the reflected shock passes back though the material interface.

B. Asymmetric Target: [Fig. 2(b)]

In this configuration, differences in shock velocity for Sn and acrylic (Fig. 12) combined with the varying thickness of the acrylic alter the initially cylindrical shock propagation and shift the center of convergence. As for the symmetric target, shock and interface trajectories are compared along with measurements of the shock convergence location. Trajectory information is compared along 0° and 180° chords located through the thin and thick sides of the outer tin target.

Fig. 13 shows that RAGE simulations and experimentally measured shock positions follow the same data trends seen in the previous symmetrical case. Very good agreement in the form of the trajectory is seen but the simulated shocks lead the radiographic data by approximately 100 ns. A 2-D comparison of simulated and radiographic shock location is presented in Fig. 14. The underlying image is a static radiograph from NTLX-2 before liner/target impact has occurred. Simulated and radiographic data of the shock boundaries from the NTLX-2 shot are then overlaid on the static image with dashed and solid lines. The experimental times of the shock boundaries are at 14.21, 14.93, and 15.58 μs. The timing for the simulated data is arbitrarily adjusted by 104 ns in order to compare the shape of the shock boundary. By adjusting the relative timing between simulation and experiment, it is possible to obtain

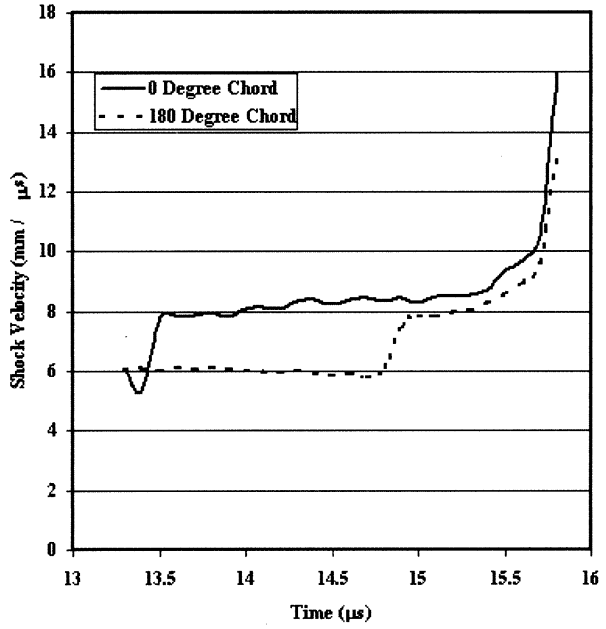

Fig. 12. Shock velocities as calculated by RAGE exhibit shock acceleration on passage through the interface boundary. Shock velocities in this experiment are approximately 6 mm/μs in tin and 8 mm/μs in acrylic. Area convergence effects dominate during the last several millimeters of the run-in producing the observed shock acceleration.

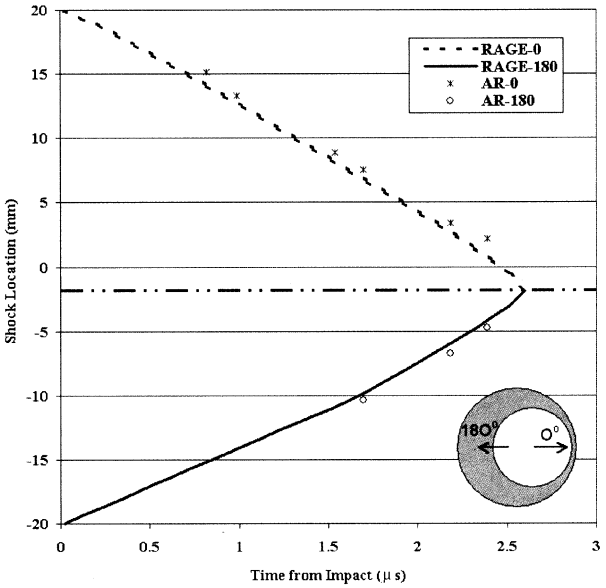

Fig. 13. RAGE simulations of the asymmetric target show a good level of agreement in the behavior of the trajectory. However, simulation results consistently lead radiographic data by roughly 100 ns.

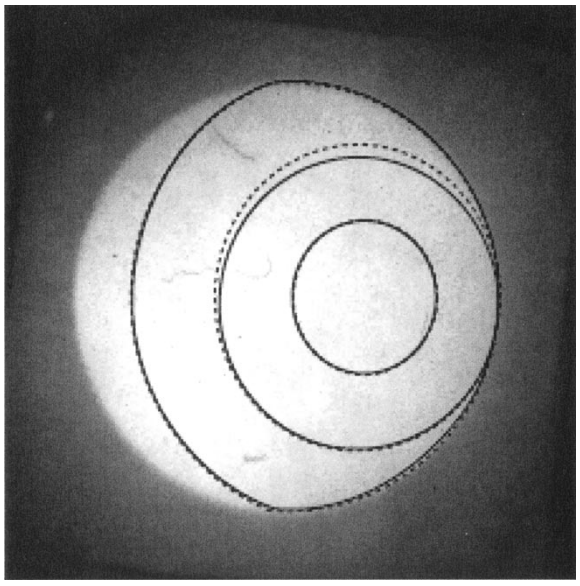

Fig. 14. Simulated (- - -) and radiographic (——) shock trajectories are compared in 2-D after applying an arbitrary timing correction of 104 ns to the simulated results.

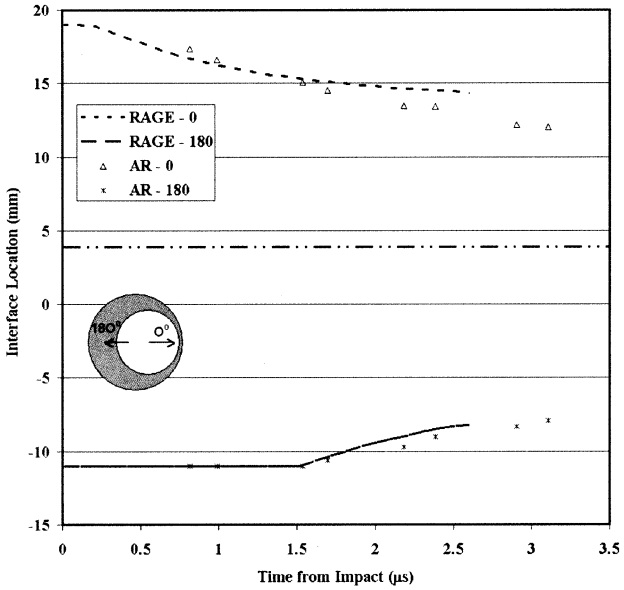

Fig. 15. Calculated interface behavior is similar to the symmetric target with the simulation initially predicting a higher rate of compression. A higher level of disagreement is seen on the thin side of the outer tin target.

excellent agreement in the shock location for the first and last radiographic frames. In the second frame at 14.93 μs, the radiographic image appears to exhibit a higher degree of distortion than either the first or third frame. The distortion in frame 2 is presumed to exist within the radiographic image since a uniform liner implosion will produce a shock symmetric about the image mid-plane. Radiographic frames 1 and 3, as well as the simulated data clearly shows the high degree of symmetry missing from radiographic frame 2. The center of shock convergence also shows an excellent agreement between simulation and experiment with centers of convergence measured at (−1.875 mm, 0.0) and (−1.808 mm, 0.0), respectively, from Fig. 14.

Sn/acrylic interface locations for the asymmetric target are displayed in Fig. 15. As previously seen in the symmetric target, RAGE simulations of the material interface exhibit similar trends to the radiographic data with a slightly higher initial interface velocity. A larger discrepancy is observed along the 0° chord where the outer tin layer is only 1 mm thick. This may indicate that either strength or equation-of-state issues associated with the polymer nature of the inner acrylic target are producing a more complex interface behavior than

expected. In comparisons for the symmetric target, similar behavior was observed with both RAGE and RAVEN producing identical results. Since RAVEN includes a strength model and RAGE did not, this appears to indicate that inaccuracies in the equation-of-state data at these high shock pressures would be a more likely culprit for differences in the interface position. It is also possible that the rapid slowing of the calculated interface is due to an overestimation of the effect of the release wave as it passes through the interface. However, simulations of the symmetric target show that this effect occurs in both RAVEN and RAGE, which produce identical results but are based on different solution techniques.

V. Conclusion

With the increased interest in using numerical simulation as a predictive tool, it is necessary to ensure that there exists a sufficient level of confidence in general use codes. This means that these tools must be capable of simulating relatively simple, let alone, more complex experiments. These efforts were focused on the design and comparison of the NTLX experimental series using the RAVEN and RAGE codes at Los Alamos National Laboratory. Throughout the NTLX series, RAVEN and RAGE show excellent agreement, yet both codes predict results that differ from experimental observations.

In the acrylic core of the target, simulated and experimental shock locations appear to have a similar radial velocity, but the simulated shock consistently arrives approximately 100 ns earlier at any given radial location. Experimental determination of impact timing was shown to be a complex issue in that the B-dot probes employed provide only an indirect measurement of the actual collision. Liner impacts are also not instantaneous in that it takes between 26–123 ns to complete a collision in the NTLX series. In conjunction with experimental timing uncertainties on the order of tens of nanoseconds, this indicates that we are near the experimental limit in terms of absolute timing comparisons for trajectory information. Relative timing differences on the order of 100 ns should be expected in future hydrofeature shock experiments. However, it may be possible to reduce this uncertainty through an effort to better characterize the physics of liner/target interactions and the generation of the subsequent B-dot signal. Utilizing a series of surface pin probes along with the current B-dot loops on a future experiment would allow benchmarking of the inherent delay between liner/target impact and generation of a B-dot signal.

Discrepancies in the location of the Sn/acrylic boundary indicate a greater degree of uncertainty in the calculated material behavior than that seen for the shock calculations. Code results are self-consistent and appear to indicate that strength issues are not important, yet both results disagree with experimental measurements. Computationally, equation-of-state issues are being explored to attempt to align the simulated and measured data. A second experimental series is also currently underway at the Atlas Pulsed Power Machine at the Los Alamos National Laboratory. This experimental series will consist of five targets with geometries identical to those used on NTLX. The materials will be varied to further explore strength and EOS effects by keeping the outer Sn target and replacing the inner acrylic target with water. Water was chosen as a working fluid since it has a well-studied EOS, has no associated strength, and will ease manufacturing of more complex geometries.

Acknowledgment

The authors wish to thank the staff of the Weapons Laboratory at Kirtland AFB for operational support of Shiva Star and making the NTLX series a success.

References

[1] W. L. Baker, J. D. Beason, G. Bird, C. B. Boyer, J. S. Buff, S. K. Coffey, J. F. Davis, J. H. Degnan, M. H. Frese, J. D. Graham, K. E. Hackett, D. J. Hall, J. L. Holmes, E. A. Lopez, R. E. Peterkin, N. F. Roderick, S. W. Seiler, and P. J. Turchi, "Plasma flow switch driven implosions," *Megagauss Fields Pulsed Power Syst.*, pp. 615–622, 1990.

[2] R. M. Baltrusaitis, M. L. Gittings, R. P. Weaver, R. F. Benjamin, and J. M. Budzinski, "Simulation of shock-generated instabilities," *Phys. Fluids*, vol. 8, pp. 2471–2483, Sept. 1996.

[3] R. L. Holmes, G. Dimonte, B. Fryxell, M. L. Gittings, J. W. Grove, M. Schneider, D. H. Sharp, A. L. Velikovich, R. P. Weaver, and Q. Zhang, "Richtmyer–Meshkov instability growth: Experiment, simulation and theory," *J. Fluid Mech.*, vol. 389, pp. 55–79, June 1999.

[4] T. A. Oliphant, *RAVEN Physics Manual*. Los Alamos, NM: Los Alamos National Laboratory, 1981, LA-8802-M.

[5] T. A. Oliphant and K. H. Witte, *RAVEN*. Los Alamos, NM: Los Alamos National Laboratory, 1987, LA-10 826.

[6] R. L. Bowers, J. H. Brownell, H. Lee, K. D. McLenithan, A. J. Scannapieco, and W. R. Shanahan, "Design and modeling of precision solid liner experiments on Pegasus," *J. Appl. Phys.*, vol. 83, pp. 4146–4159, Apr. 1998.

[7] S. P. Lyon and J. D. Johnson, *SESAME: The Los Alamos National Laboratory Equation of State Database*. Los Alamos, NM: Los Alamos National Laboratory, 1992, LA-UR-92-3407.

[8] D. J. Steinberg, S. G. Cochran, and M. W. Guinan, "A constitutive model for metals applicable at high-strain rate," *J. Appl. Phys.*, vol. 51, pp. 1498–1504, Mar. 1980.

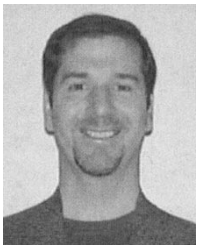

Randall J. Kanzleiter received the Ph.D. degree in engineering physics from Rensselaer Polytechnic Institute, Troy, NY, in 1999.

He served as a Post-Doctoral Researcher at the Los Alamos National Laboratory performing hydrodynamic code validation experiments at the Shiva Star Pulsed Power Facility, Kirtland AFB, Albuquerque, NM. In 2001, he became a Technical Staff Member at Los Alamos National Laboratory, Los Alamos, NM. His current research interests include studies of shock physics and modeling hydrodynamic phenomena in convergent geometries.

Walter L. Atchison received the B.S. degree in nuclear engineering from the University of Tennessee, Knoxville, the M.S. degree in physics from the University of New Mexico, Albuquerque, and the Ph.D. degree in engineering applied science from the University of California, Davis, CA, in 1975, 1979, and 1990, respectively.

In 1994, he retired from the Air Force and began working at the Los Alamos National Laboratory, Los Alamos, NM, performing design and analysis of experiments in support of the Nuclear Weapons Technology Program. These experiments focused on hydrodynamic code validation experiments using the PEGASUS and ATLAS facilities, as well as explosive pulse power systems. His current research interests include studies of shock physics, modeling hydrodynamic phenomena in convergent geometries, and material properties.

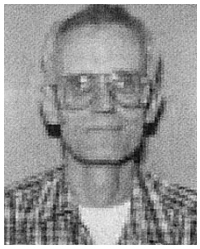

Richard L. Bowers received the M.A. degree from Occidental College, Los Angeles, CA, and the M.S. and Ph.D. degrees in theoretical physics from the University of Oregon, Eugene, in 1963, 1967, and 1971, respectively.

From 1971 to 1976, he was been a member of the Center for Relativity Theory and the Center for Particle Theory at the University of Texas at Austin doing research in astrophysics. After a year at Bell Laboratories, he joined Lawrence Livermore National Laboratory, Livermore, CA, working in applied and computational physics (1977–1982). Since 1982, he has been a member of the Applied Theoretical Physics Division at Los Alamos Laboratory, Los Alamos, NM, working on computational modeling and pulsed power applications.

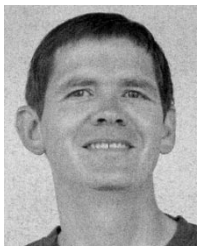

Richard L. Fortson received the B.S. degree in meteorology from Texas A&M University, College Station, and the M.S. degree in civil engineering (photogrammetry) from Purdue University, W. Lafayette, IN, in 1980 and 1983, respectively.

In 1987, he joined the Los Alamos National Laboratory, Los Alamos, NM, as a Technical Staff Member in the International Technology (IT) Division. While in IT, he worked on image processing projects concerning issues of national security. Previous to coming to Los Alamos, he served on the technical staff at the Defense Mapping Agency Aerospace Center, St. Louis, MO, working in the areas of image processing, digital cartographic mapping, and sensor simulations. He is currently serving as a technical staff member in the Modeling, Algorithms, and Informatics Group (CCS-3) at Los Alamos. His primary interests are in the areas of image processing and pattern recognition. He is currently working with the NNSA's ASCI (Accelerated Strategic Computing Initiative) project, where is he devising methods for detecting anomalous features in large 3-D hydrocode simulation data sets.

Joyce A. Guzik received the B.A. degree in physics, mathematics, and Russian studies from Cornell College, Mt. Vernon, IA, and the Ph.D. degree in astrophysics from Iowa State University, Ames, in 1982 and 1988, respectively.

She is currently a Technical Staff Member at Los Alamos National Laboratory, Los Alamos, NM, and continues her involvement in astrophysics research, specializing in numerical modeling of stellar evolution and pulsation. She is the co-author of 27 refereed articles in astrophysics journals and over 100 contributed and invited conference papers. She has served on a number of technical review committees, including those for the Laboratory Directed Research and Development program, the National Ignition Facility, the Sandia Z machine, and the ASCI Academic Strategic Alliance Program.

Dr. Guzik has been awarded a UC Santa Barbara Institute for Theoretical Physics visiting Fellowship for 2001–2003.

Russell T. Olson, photograph and biography not available at the time of publication.

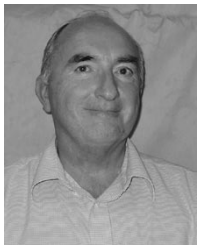

John L. Stokes received the B.S. degree in physics from Weber State College, Ogden, UT, in 1966, and the Ph.D. degree in solid-state physics from Brigham Young University, Provo, UT, in 1972.

He has been with the Los Alamos National Laboratory (LANL), Los Alamos, NM, for his entire career, performing research in both experimental and computational physics. His areas of research include fission and thermonuclear fusion, and calculation and development of diagnostic techniques including high-precision optically-based current measurements in the hostile pulsed-power environments. For the past decade, his research emphasis has been on the application of pulsed power for cylindrical implosions using the Pegasus and Atlas Facilities, LANL, as well as explosive pulsed-power systems.

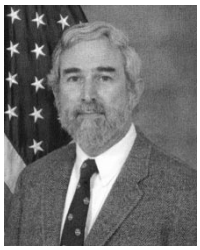

Peter J. Turchi (SM'84–F'00) was born in New York City on December 30, 1946. He received the B.S.E., M.A., and Ph.D. degrees in aerospace and mechanical sciences from Princeton University, Princeton, NJ, in 1967, 1969, and 1970, respectively.

Assigned to active duty as an Air Force officer at the Air Force Weapons Laboratory, Kirtland AFB, NM, he initiated (with W. L. Baker) in 1971, the Shiva program for generating megajoules of soft X-rays by electromagnetic implosion of high atomic-number plasma shells. From 1972 to 1980, as a civilian scientist at the Naval Research Laboratory, Washington, DC, he designed and operated imploding liner systems for controlled thermonuclear fusion at megagauss magnetic field levels (NRL Linus program), culminating in the successful demonstration of repetitive, stabilized implosions of liquid-metal liners. He also served (1977–1980) as Chief of the Plasma Technology Branch. From 1980 to 1989, he was a Senior Research Scientist at R&D Associates, Inc. As Director of its Washington Research Laboratory in Alexandria, VA, he led the successful effort to switch megajoules of magnetic energy at 12 MA using pulsed-plasma flows. He left private industry in 1989 for ten years as a Professor of Aerospace Engineering at The Ohio State University, Columbus, during which time he also served as visiting Chief Scientist for Advanced Weapons and Survivability at the United States Air Force Phillips Laboratory, Kirtland AFB. In 1999, he joined Los Alamos National Laboratory, Los Alamos, NM, where he led activities in hydrodynamics and pulsed power physics, including the first liner implosion experiments on the Atlas pulsed power system at 15–20 MA. Presently, as a member of the Air Force's scientific and professional cadre of senior executives, he is Senior Scientist for high-power microwaves and pulsed power at the Air Force Research Laboratory, Kirtland AFB, NM.

Dr. Turchi re-established the International Conference on Megagauss Magnetic Field Generation and Related Topics in 1979. He has served as Technical Program Chairman and General Chairman, respectively, for the Fifth and Sixth IEEE Pulsed Power Conferences, and as a member of the Executive Committee of the Plasma Science and Applications Committee. In 1999, he received the IEEE Erwin Marx Award for technical contributions to pulsed power science and technology over an extended period of time. Currently, he is President of the Electric Rocket Propulsion Society, and a member and past Chairman of both the AIAA Electric Propulsion Technical Committee and the IEEE Standing Committee on Pulsed Power Science and Technology.